Xu, W.-J., Hu, R.-L. & Tan, R.-J. (2007). *Géotechnique* **57**, No. 3, 255–264 [**doi:** 10.1680/geot.2007.57.3.255]

Some geomechanical properties of soil–rock mixtures in the Hutiao Gorge area, China

W.-J. XU*, R.-L. HU* and R.-J. TAN*

Soil–rock mixtures, which are complicated inhomogeneous materials, are widely encountered in geotechnical engineering projects. In situ tests were performed on six samples of soil–rock mixtures in the Hutiao Gorge reservoir area to examine their mechanical characteristics. The deformation behaviour of the mixtures is found to be closely related to the weight proportion of rock fragments and their size distribution, indicating that there may be critical fragment sizes that influence their mechanical properties, particularly cohesion. The soil–rock mixtures are sensitive to water. The results of the comparison between tests at natural moisture contents and under conditions of simulated rainfall give useful measured data for engineering evaluation and design. For natural soil–rock mixtures the cohesion c was 1·53 kPa and the internal friction angle ϕ was 46·0°; for saturated soil–rock mixtures c was 0·30 kPa and ϕ was 59·2°.

KEYWORDS: in situ testing; landslides; shear strength

Les mélanges terre-roche, qui représentent des matériaux inhomogènes particulièrement complexes, se rencontrent fréquemment dans les projets d'ingénierie géotechnique. Cet article décrit des tests réalisés in situ sur six échantillons de mélanges terre-roche, dans la région de la réserve de la gorge Hutiao, pour étudier leurs propriétés mécaniques. Le comportement des mélanges à la déformation est étroitement liée à la proportion en poids des fragments de roche et à leur distribution en taille, indiquant ainsi qu'il peut exister des dimensions de fragments critiques qui influencent leurs propriétés mécaniques, en particulier leur cohésion. Les mélanges terre-roche sont sensibles à l'eau. Les résultats de la comparaison entre les essais réalisés avec une teneur en humidité naturelle et dans des conditions de pluie simulée permettent d'obtenir des mesures utiles pour la conception et l'évaluation technique. Pour les mélanges terre-roche naturels, la cohésion c était de 1,53 kPa et l'angle de frottement interne ϕ de 46,08°; pour les mélanges terre-roche saturés, c était de 0,30 kPa et ϕ de 59,28°.

INTRODUCTION

Soil–rock mixtures consist of rock blocks within soil composed of sand, silt and clay (Fig. 1). The geological origins of soil–rock mixtures vary between landslide deposits, colluvial deposits, alluvial-diluvial deposits and glacial deposits. Soil–rock mixtures have geomechanical and other characteristics different from those of pure rock or soil masses. Medley (1994) incorporated this kind of mélange into 'bimrock' (block-in-matrix rocks), which means 'geological mixtures composed of geotechnically significant rock blocks within a bonded rock matrix of finer texture'. Soil–rock mixtures are widespread in southwest China. For example, in the west of Sichuan Province 61·3% of slopes are composed of soil–rock mixtures (He, 2004). Many large-scale landslides are made up of soil–rock mixtures. An example is the Xintan landslide of the Three-Gorge region of the Yangtze River, China, which slid on 12 June 1985 (Xia & Zhu, 1996). Another example is the Youpingzui landslide in Yibin city (a city of Sichuan Province, China), which slid on 30 June 2004. The behaviour of these slopes has a huge influence on engineering projects and on people's lives.

With the development of all kinds of large-scale engineering projects, the stability of some engineering geological bodies (such as slopes, foundations, and rock adjoining tunnels) is controlled mostly by the mechanical properties of the soil–rock mixtures distributed in the engineering area. During the last few decades, the study of the geometrical and mechanical features of soil–rock mixtures has attracted

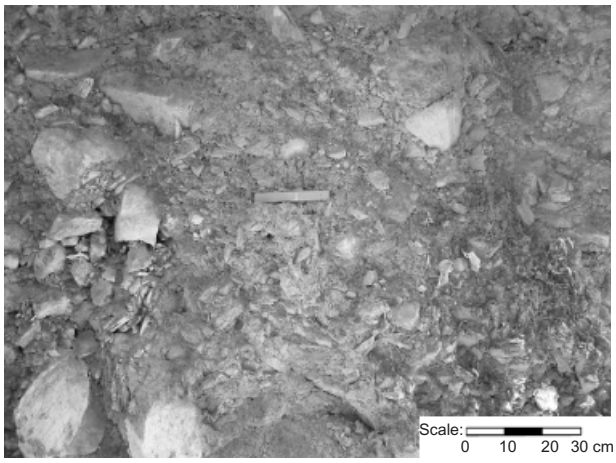

Fig. 1. Photograph of soil–rock mixtures in Hutiao Gorge, China

Manuscript received 22 March 2005; revised manuscript accepted 11 October 2006.
Discussion on this paper closes on 1 September 2007, for further details see p. ii.
* Key Laboratory of Engineering Geomechanics, Institute of Geology and Geophysics, Chinese Academy of Sciences, Beijing, China.

increasing attention. Vallejo & Zhou (1994) and Iannacchione (1997) carried out many tests to study the mechanical properties of both saturated clays containing rock particles and simulated soil–rock mixtures, and concluded that the shear strength of unsaturated and saturated clay was altered by floating, oversized rock particles. Through triaxial tests on physical models of mélanges, Lindquist & Goodman (1994) indicated that the strength and deformation properties of mélanges were significantly affected by volumetric block proportion and fabric orientation. Based on the porosity of soil–rock mixtures and the type of structural support provided by coarse and fine grains, Vallejo & Mawby (2000) and Vallejo (2001) studied the influence of the weight concentration of rock fragments on the shear strength of granular material-clay and binary granular mixtures. Li & Wang (2004) presented a stochastic model for soil–rock mixtures on the basis of Monte Carlo random sampling. They used the discrete element method to examine the influence of factors such as rock size on the distribution of stress fields in soil–rock mixtures under uniaxial compression. According to these studies, it is believed that the internal structure of soil–rock mixtures and the weight percentage of rock fragments significantly influences their mechanical properties and failure mechanisms.

To date, there has been little study of the physical and mechanical properties of soil–rock mixtures. A review of the available publications show that there have been very few field tests of the mechanical properties of soil–rock mixtures, and analyses of the mechanical properties of soil–rock mixtures based on their granulometric composition are also limited. There is no literature that can be found about the mechanical properties of soil–rock mixtures subjected to rainfall, which are very important for studying the stability of soil–rock mixture landslides.

The Hutiao Gorge, Jinsha River, China was chosen as a testing area to study the geomechanical properties of soil–rock mixtures. Six in situ shear tests were performed. Three were performed under natural conditions and three under simulated rain conditions. Grain-size analyses, calculation of strength parameters (c and ϕ), soil–rock mixtures and analyses of the 3D sliding planes were also performed. Based on these analyses, the strength parameters (c and ϕ) of the soil–rock mixture in the study area are presented, and conclusions drawn about the geotechnical properties of soil–rock mixtures.

DESCRIPTION OF TEST SITES

The study area is located at the Longpan landslide in Longpan County, Lijiang City, Yunnan Province, south-west China, at the right bank of the Hutiao Gorge reservoir area (Fig. 2). The elevation of the landslide is between 1820 m and 2240 m. Field investigation shows that the soil–rock mixture is between 5 m and 40 m thick, and consists of rock fragments and minor clay. The geological origin of the soil–rock mixtures in this area is landslide deposits. The rock fragments in this area are mainly 1–5 cm in size (Fig. 1), and are composed mostly of irregular-shaped sandstone and slate fragments.

The six test sites are near Longpan tunnel No. 1, where

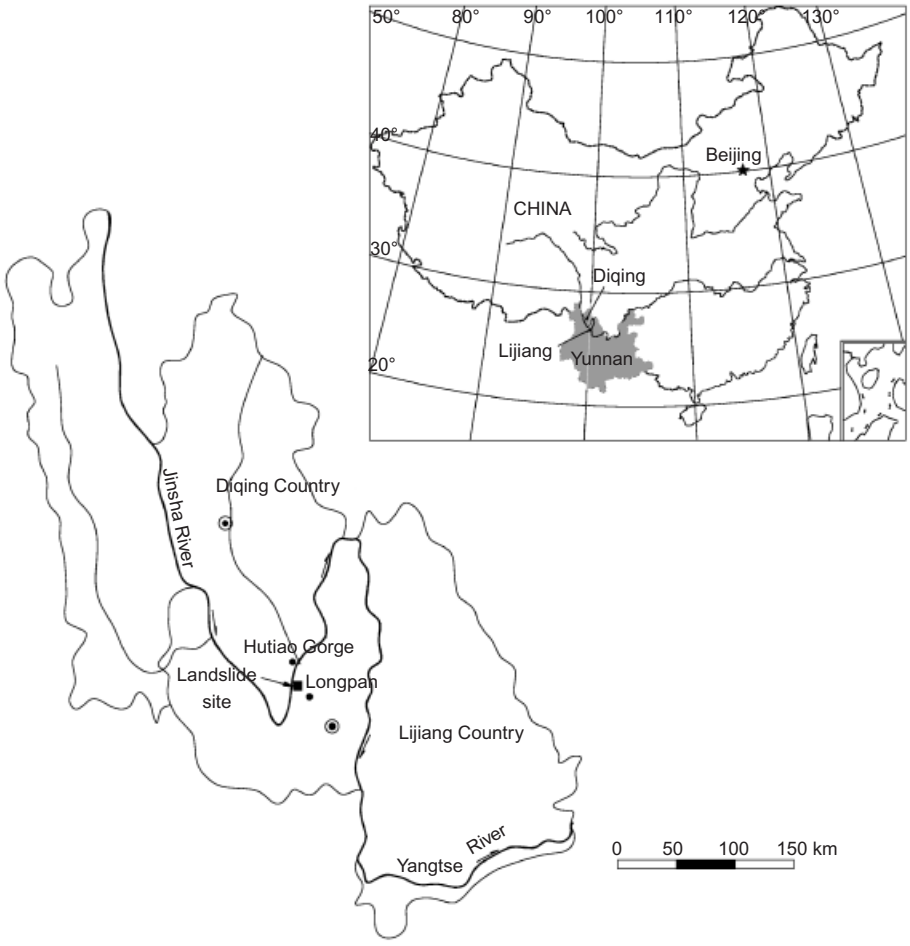

Fig. 2. Location map of the study area

the soil–rock mixtures are typical of the Hutiao Gorge reservoir area. The elevation of these sites is about 1892 m (Fig. 3). The six test sites were divided into two sets. The tests at sites 1, 2 and 3 were performed under natural conditions, whereas the tests at sites 4, 5 and 6 were performed under simulated rain states to provide comparative data necessary for engineering evaluation and design. The test sites were located near each other to ensure that the weight proportion of rock and the texture of the soil–rock mixtures were approximately the same between the two sets, thereby allowing comparison between the two test sites.

IN SITU TEST PROCEDURE

Preparation of test samples

In situ shear test samples were prepared at each site. The size of each test sample had to meet two criteria: its height was five times larger than the maximum fragment diameter, and its width/height ratio was about 3 to 4. All six test samples were about 80 cm long by 80 cm wide by 30 cm high. The test samples were prepared as follows (Fig. 4).

(*a*) Three trenches were excavated around the test sample, one at the front and the others at the sides. The front trench was used to set up the test equipment (such as a jack), and its width depended on the dimensions of the test equipment. The two lateral trenches were about 20 cm and 1·5 m wide respectively, the latter used to observe the deformation.

(*b*) Following excavation, the unit weight and particle size distribution of the excavated materials were measured, and the excavated sections photographed.

(*c*) The three exposed faces of the test sample were covered with clay, 0·5 cm thick, to make them even and smooth.

(*d*) A 5 cm spacing grid was plotted on the top and side surfaces of the test sample to determine and measure the sliding surfaces.

(*e*) A steel plate was placed vertically into the 20 cm wide lateral trench, against the test sample, and clay was placed and tamped in the remainder of the trench to separate the test sample from the surrounding soil–rock mixture. The surface of the steel plate facing the test sample was coated with petroleum jelly to decrease friction.

(*f*) A 2 cm thick Plexiglass plate was placed against the face of the test sample in the 1·5 m wide trench, and was secured by steel stakes and tie bars to prevent its lateral displacement. The face of the Plexiglass facing the test sample was coated with petroleum jelly to decrease friction.

(*g*) A steel plate, with its inside face coated with petroleum jelly, a wood block and the test equipment, a jack, a large-range dial indicator and an oil manometer, were placed in front of the test sample in that order. The centre of the piston of the jack was maintained in line with a point located at half of the width and one third of the height of the steel plate.

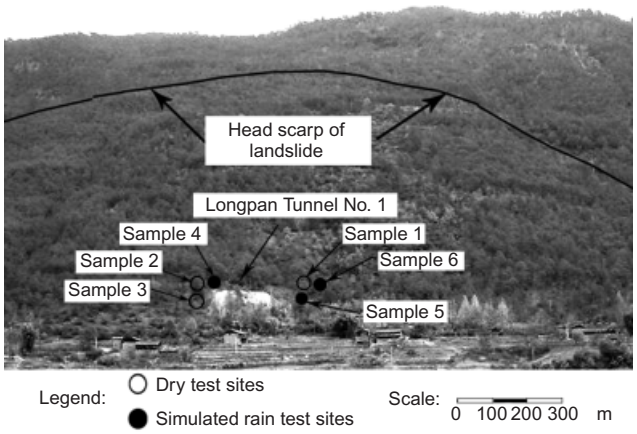

Fig. 3. Distribution of test samples

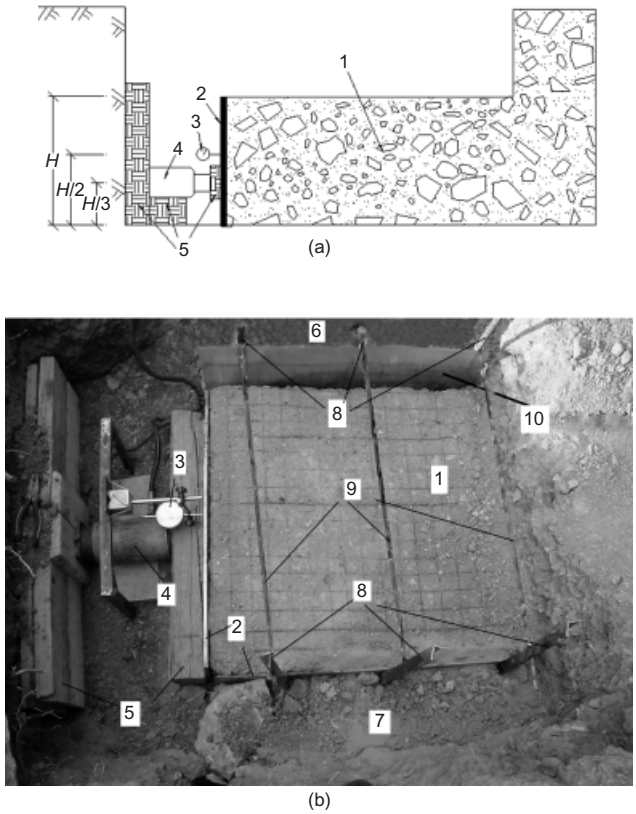

Fig. 4. Arrangement of the in situ shear tests: (a) profile of test sample; (b) view from above (1, test sample; 2, steel plates; 3, dial indicator; 4, jacks; 5, cross-tie; 6, observation position; 7, sealed earth; 8, steel stakes; 9, tie bar; 10, Plexiglass plate)

Testing

For the tests under natural conditions, a shearing deformation rate of about 2 mm/15–20 s was maintained, while continual recording of the shear displacement (shown on the dial gauge) and hydraulic pressure in the jack (indicated by the oil manometer) took place. When the hydraulic pressure reading reached a maximum (i.e. continued shearing would require reduced pressure), the maximum shear force P_{max} was recorded and the hydraulic pressure released. Once the hydraulic pressure had dropped to a relatively stable value, the shear force was re-applied. When the reading of the oil manometer reached another maximum, this was recorded as the minimum shear force, P_{min}.

For the simulated rain tests, water was sprayed continuously and uniformly on the top surface of the sample for about 2–3 h before testing. The appropriate time for spraying water was estimated from the hydraulic conductivity of the soil–rock mixtures and by testing nearby samples. In these tests the water-spraying rate was 65 l/h and the spraying duration was about 2·5 h. The test loading procedure was the same as for the natural tests, except that water was sprayed throughout the test process to maintain

standing water on the top surface of the test sample. In the last phase of the test fractures had developed, and the hydraulic conductivity increased: therefore the rate of water-spraying was appropriately increased.

Post-testing procedures

After the test, the testing equipment was removed and the position of the fracture surfaces was defined by drawing a sketch map of the sliding plane. For the simulated rain tests, a sample was immediately removed after testing to determine the unit weight and the water saturation of the soil–rock mixture.

For both test conditions, one or two days after the initial test, the sample was reloaded without the lateral restraint to observe the behaviour of the major sliding planes. The jack was then removed and the upper sliding body of the test sample removed to expose the major sliding plane for each test sample. A sketch of each 3D failure surface was drawn.

RESULTS AND ANALYSES

Particle size distribution

Particle size distribution analyses were performed for test samples 1, 2 and 3. (As test sample 4 was located close to sample 2, and test samples 5 and 6 were located close to sample 1, their particle size distributions, as measured in situ, were similar: therefore only the particle size distributions of test samples 1, 2 and 3 are described in this paper.) The masses of the samples were approximately 24·2 kg for sample 1, 27·1 kg for sample 2, and 19·6 kg for sample 3. The results of the particle size analyses (Fig. 5) indicate that the soil–rock mixtures were well graded: the coefficient of uniformity C_u was 50 and the coefficient of curvature C_c was about 5·7 (Fig. 5(b)). The percentage by weight of the finer materials with grain diameter less than 15 mm in the samples was greater than 45%, and some were even as high as 62%, such as test site No. 3. The average grain diameter was 14 mm.

Any reasonable dimension can be used to scale the soil–rock mixtures because of the scale independence. It is important to select a reasonable threshold size between soil and rock at the scale of the test. Medley called such a descriptive length the characteristic engineering dimension L_c (Medley, 1994; Medley & Lindquist, 1995), and suggested 5% of L_c as the soil–rock threshold. Here, we took the height of the test sample as the characteristic engineering dimension L_c. The soil–rock threshold of the test sample at the scale of the test should be $0{\cdot}05 \times 300\ \text{mm} = 15\ \text{mm}$. Therefore in this paper 'rock' means blocks with dimensions greater than 15 mm. According to this soil–rock threshold, the weight proportions of rock of test samples 1, 2 and 3 were 56%, 54% and 37% respectively.

Although soil–rock mixtures are a typical inhomogeneous geomaterial, and the distribution of the internal rock fragments is very stochastic, they have the favourable character of self-comparability in statistics. Scale-independence is an important characteristic of soil–rock mixtures (Medley & Lindquist, 1995; Xu & Hu, 2006). The local concentration of rock fragments in soil–rock mixtures has little impact on

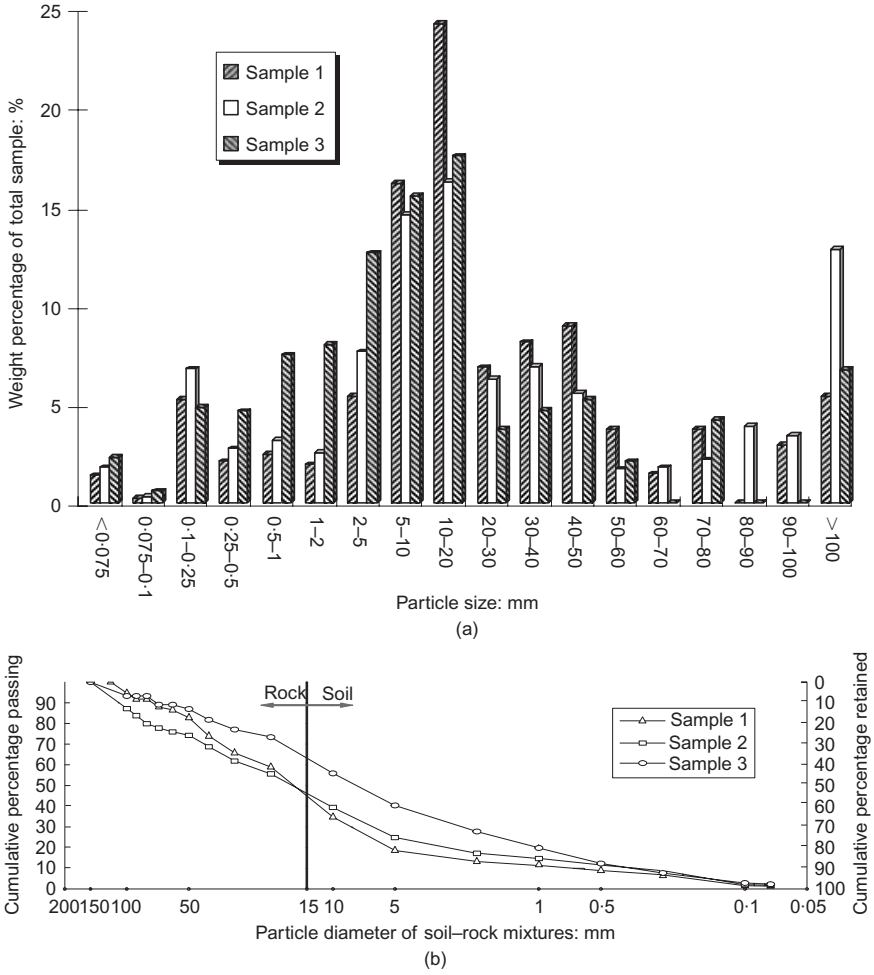

Fig. 5. Grain-size analyses for test sites 1, 2 and 3: (a) histogram showing weight percentages of various size fractions; (b) grain size distribution curves

the uniform statistical distribution of the fragments in the whole test sample. Therefore the percentage by weight of rock fragments in the mixtures obtained through sieve analysis can be used to characterise the material, not the local percentage by weight of rock fragments.

Previous research (Lindquist & Goodman, 1994; Vallejo & Mawby, 2000; Vallejo, 2001) has indicated that when the weight proportion of rock fragments in soil–rock mixtures is more than 75%, the shear strength of the mixture is controlled by the rock fragments alone. However, when the percentage by weight of rock fragments in the mixture was less than 40%, the shear strength of the mixture is controlled by the finer materials (or soils). In this study area, the percentage by weight of rock fragments of the test samples is between 40% and 75%. Therefore it can be concluded that the shear strength of the mixture was controlled both by the rock fragments and by the finer materials.

Average sliding plane

The three-dimensional failure surfaces in the test samples were very irregular (Fig. 6), and in order to obtain more accurate strength parameters, profiles were performed at 10 cm intervals across the surface. By averaging all these profiles, we obtained a composite, average sliding plane for every test sample. The average sliding planes for the test samples are shown in Figs 7(a) and 7(b). The average sliding surfaces zigzag irregularly. By identifying the 'turning point' of each limb of the profiles, the sliding surface was divided into several sections, which were used to calculate the strength parameters (c and ϕ) of the soil–rock mixtures.

Calculation of strength parameters c and ϕ

For the natural tests, we used the formulae provided by Lin (1994). For the simulated rain tests, to consider the effect of water pressure, we modified Lin's formulae into (Fig. 8)

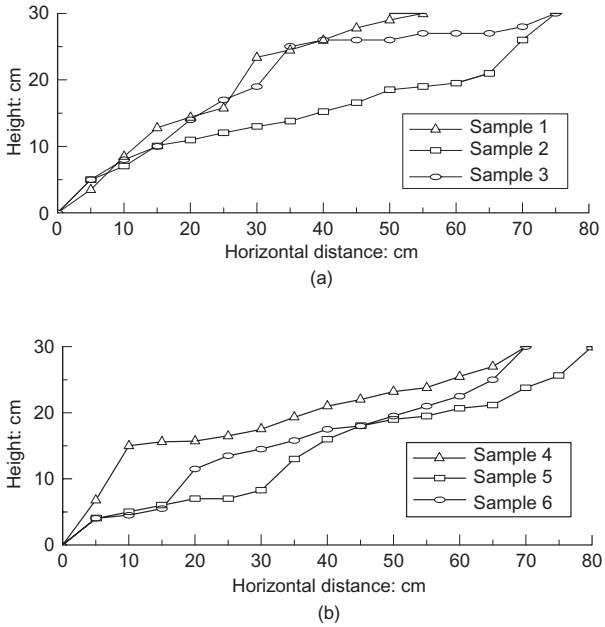

Fig. 7. Profiles of average sliding surfaces for the test samples: (a) natural samples; (b) simulated-rain test

$$c = \frac{P_{\max} - P_{\min}}{\sum_{i=1}^{n} L_i \cos \alpha_i} \tag{1}$$

$$\tan \phi = \frac{(P_{\max}/G)\sum_{i=1}^{n} g_i \cos \alpha_i - \sum_{i=1}^{n} g_i \sin \alpha_i - c\sum_{i=1}^{n} l_i}{(P_{\max}/G)\sum_{i=1}^{n} g_i \sin \alpha_i + \sum_{i=1}^{n} g_i \cos \alpha_i - \sum_{i=1}^{n} W_i} \tag{2}$$

where ϕ is the internal friction angle (degrees); c is the cohesion (kPa); $P_{\max}$ is the maximum shear force (kN); $P_{\min}$

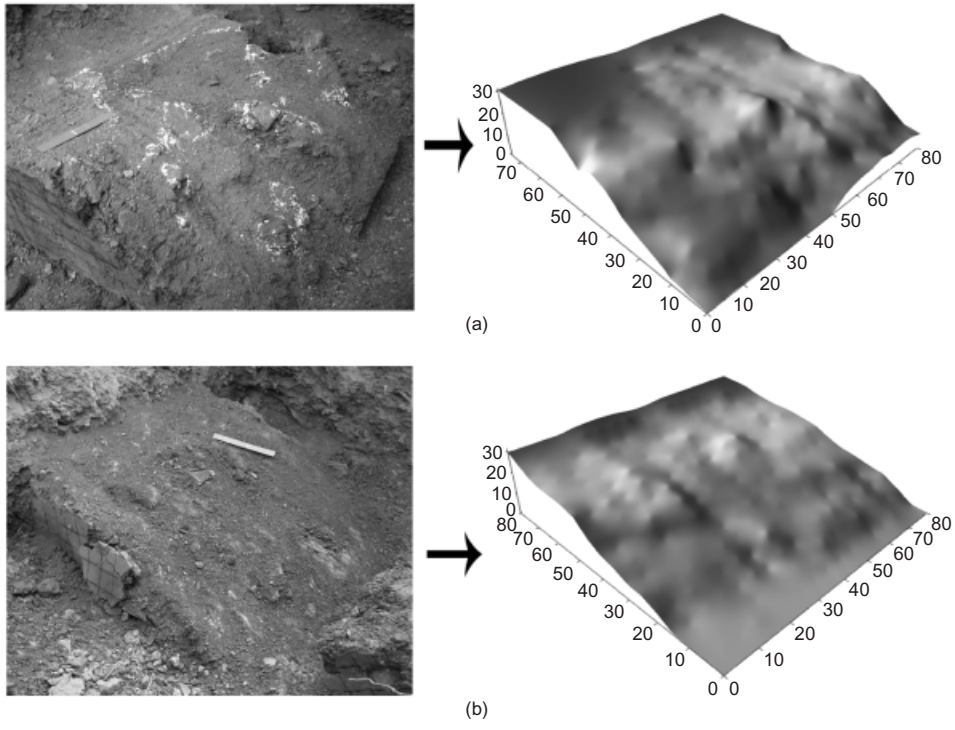

Fig. 6. Major 3D sliding surfaces of: (a) test sample 1; (b) test sample 3

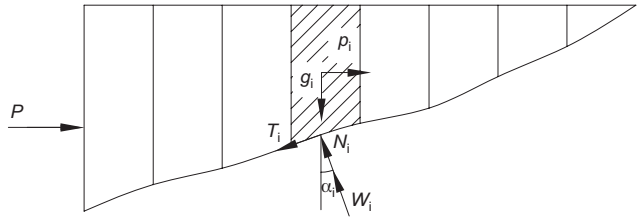

Fig. 8. Profile of sliding body and its loading analysis

is the minimum shear force (kN); G is the weight of the sliding mass body (kN); α_i is the angle between the sliding plane and the horizontal plane of the ith sliding block; l_i is the length of the sliding line of the ith sliding block (m); g_i is the weight of the ith sliding block (kN); and W_i is the water pressure on the sliding plane of the ith sliding block (kN/m), calculated by

$$W_i = \rho_w g h_i l_i \tag{3}$$

where ρ_w is the density of water, g is the acceleration due to gravity, and h_i is the height of the midline of the ith sliding block. The calculated results for c and ϕ are listed in Table 1.

Strength characteristics of soil–rock mixtures

Natural conditions. Shear stress–displacement curves for each of samples 1, 2 and 3 are shown in Fig. 9(a). By comparing the strength parameters of each sample site, it can be seen that there is close relationship between the strength parameters of the soil–rock mixtures and their weight proportion of rock.

Test sample 1, whose weight proportion of rock is 56%, has an internal friction angle of 47·60°, and cohesion of 0·47 kPa. The weight proportion of rock of test sample 2 is 54%, which is close to that of test sample 1, and its internal friction angle is 49·02°, which is also similar to that of sample 1. However, the cohesion of sample 2 is 1·76 kPa, which is larger than that of sample 1. Sample 2 contains 16% of rock fragments 10–20 mm in size (about $0{\cdot}05L_c$ = 15 mm) sized rock fragments, which is less than sample 1 (24%), but has 13% of rock fragments larger than 100 mm, which is more than sample 1.

Test sample 3 contains 18% of 10–20 mm rock fragments, which is close to that of sample 2 (16%), but its weight proportion of rock is 37%, which is lower than that of sample 2 (54%). The internal friction angle of sample 3 is 41·24°, which is less than that of sample 2 (49·02°); however, its cohesion is 2·35 kPa, which is larger than that of sample 2.

Based on these limited observations of the soil–rock mixtures, cohesion is apparently controlled not only by the weight proportion of rock but also by the weight proportion of the blocks in a specific particle size range, termed the *key particle size*. The internal friction angle of the soil–rock mixtures is controlled mainly by the weight proportion of rock: a higher fines content (at the scale of the test) more readily facilitates shearing, resulting in lower internal friction angles.

The shear stress–shear displacement curves (Fig. 9(a)) are analogous to complete stress–strain curves obtained under axial compression. Using this analogy, these curves, which are different from those of either the general soil or the rock mass, can be divided into five stages, as follows (Fig. 10).

(*a*) *Stage O–A*. This is the compaction stage, and the stress value at point A is the compaction strength. Depending on the weight proportion of rock and the original

Table 1. Summary of results for each of the six test sites

Test	Test number	Saturation: %	Unit weight, γ: kN/m^3	Mass of sliding body, kN/m	Maximum shear force, P_{max}: kN/m	Minimum shear force, P_{min}: kN/m	$\sum_{i=1}^{n} g_i \cos\alpha_i$: kN/m	$\sum_{i=1}^{n} g_i \sin\alpha_i$: kN/m	$\sum l_i \cos\alpha_i$: m	Water pressure $\sum_{i=1}^{n} W_i$: kN/m	Strength parameters	
											c: kPa	ϕ: degrees
Natural state	1	–	17·41	1·22	7·49	7·14	1·02	0·61	0·75	–	0·47	47·60
	2	–	17·46	1·98	8·15	6·83	1·81	0·68	0·75	–	1·76	49·02
	3	–	17·89	1·34	8·37	6·61	1·14	0·64	0·75	–	2·35	41·24
Simulated-rain state	4	92	19·55	1·53	5·51	5·29	1·30	0·58	0·70	0·96	0·31	57·74
	5	89	19·65	2·47	6·61	6·39	2·29	0·75	0·80	1·35	0·28	60·21
	6	85	18·98	2·10	7·05	6·83	7·05	6·83	0·70	1·17	0·31	59·70

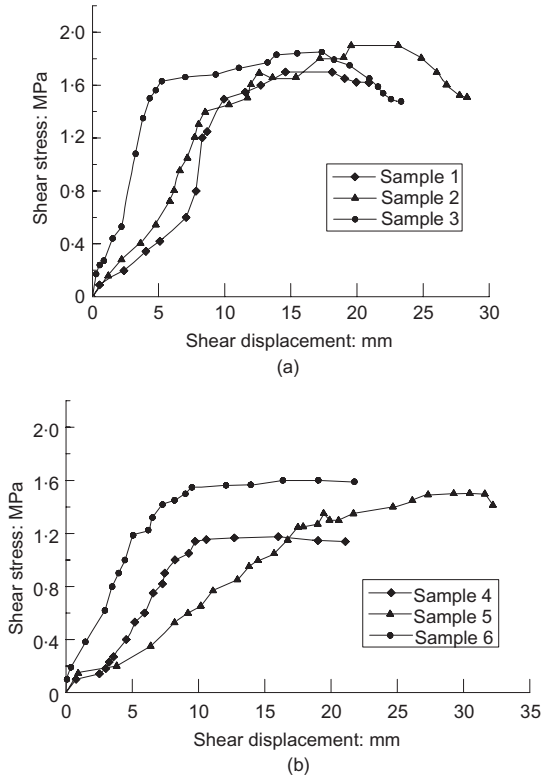

Fig. 9. Shear stress–displacement curves based on records of test samples: (a) natural test samples; (b) simulated-rain test samples

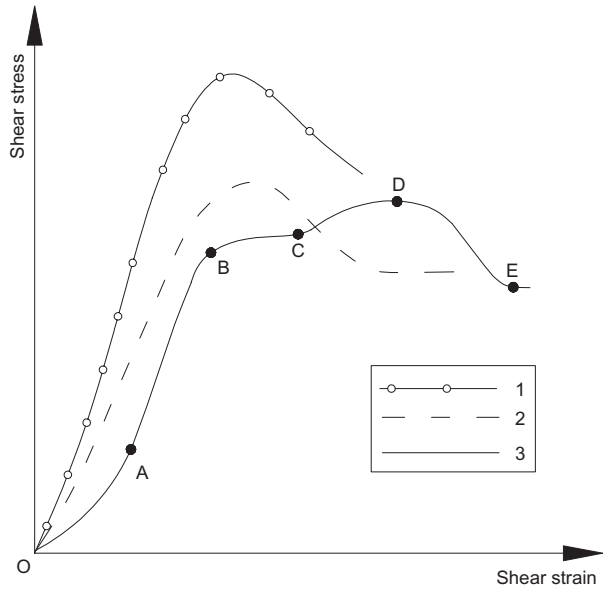

Fig. 10. Stress–strain curve for three different kinds of geomaterial: 1, typical sandstone; 2, typical overconsolidated clay; 3, soil–rock mixtures

compaction of the soil–rock mixture, curve shapes in this stage may differ significantly. When the weight proportion of rock of the soil–rock mixture is higher, or the mixture is looser, this stage is very obvious (such as for test samples 1 and 2); otherwise, it may be ambiguous (such as for test sample 3).

(*b*) *Stage A–B*. This is the elastic deformation stage, in which the stress–strain curve is close to a straight line, and the stress value at the point B is the elastic limit. The shape of the curve in this stage also depends on the weight proportion of rock, being obvious for test sample 3 (37%), but ambiguous for samples 1 (56%) and 2 (54%).

(*c*) *Stage B–C*. This is the initial yield stage, in which the matrix material (soil) of the soil–rock mixture first yields, and in some places in the test samples cracks may be generated. The stress value at point C is the yield strength. Depending on the weight proportion of rock, the curve shape in this stage may differ. When the weight proportion of rock of the sample is small, this stage may be very obvious (such as sample 3); otherwise, it may be ambiguous or even absent (such as sample 1). As shown from the curve for sample 2, when the shear force reaches 1·7 MPa there is a 'peak'. Later field investigation showed that in some locations of sample 2 the weight proportion of rock is greater, so during application of the shear force those locations are initially destroyed while the bulk of the sample remains intact.

(*d*) *Stage C–D*. This is the strain-hardening stage, in which, with the destruction of the matrix of fine-grained soil, the previously isolated stone fragments now have point-to-point contact, which leads to a strength increase of the whole test sample, followed by the propagation of cracks. The stress at point D is the ultimate strength.

(*e*) *Stage D–E*. This is the last stage of destruction. In this stage, the cracks propagate quickly until they form a continuous sliding surface. The stress at point E is the residual strength.

During the test it was observed through the Plexiglass plate that isolated cracks initially appeared, then propagated, and ultimately formed a continuous sliding surface (Figure 11). Because of the inhomogeneity of the soil–rock mixture, there were several secondary cracks that penetrated into each other during the test. Interestingly, the initial location of cracks was closely related to the distribution of the rock fragments.

Simulated rain conditions. Figure 9(b) shows curves of shear stress against displacement for test samples 4, 5 and 6. There are obvious differences between Fig. 9(a) and Fig. 9(b), which suggests that the simulated rain test samples may be deformed by a different mechanism, possibly as a result of new internal structures caused by the introduction of water into the samples.

In order to identify some of this apparent deformation mechanism, the particle size distributions were analysed before and after water spraying. The results are shown in Fig. 12, and discussed below.

From Fig. 12 it can be seen that the percentage of particles less than 0·5 mm in diameter decreased after water spraying. The porosity increased from 0·35 before spraying to 0·43 after spraying. (According to observations and measurements, only particles with dimensions less than 2 mm were carried away by the water: so this figure focuses on the size range to 2 mm. The y-coordinate of this figure is the weight percentage of particles in the size range to 2 mm. From this figure, it is found that the proportion of particles with dimensions less than 0·5 mm tends to decrease after water-spraying.)

Owing to the relatively large porosity of the soil–rock mixture and its higher permeability, the water percolates the sprayed sample, piping the finer soil. This destroys the finer soil fabric, increases the porosity of the soil–rock mixture, and influences the strength parameters of the soil matrix (at the scale of the test).

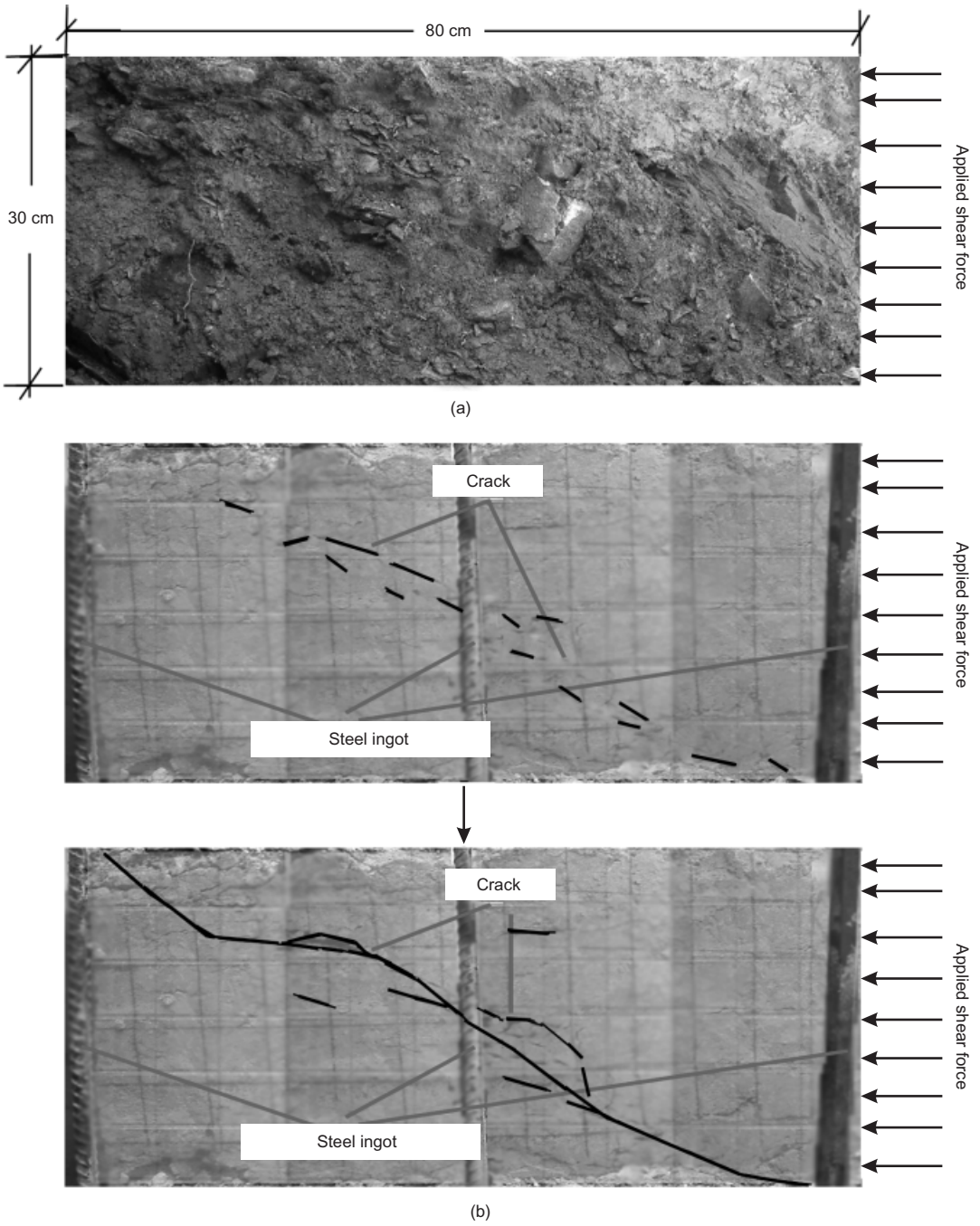

Fig. 11. Propagation of cracks in a test sample: (a) photograph of test sample's profile before testing, showing the distribution of particles; (b) same profile during the test, showing propagation of cracks with increase of shear force

Compared with the natural test samples, the maximum and minimum shear forces of the water-sprayed samples decreased (as shown in Table 1). This can be seen by comparing natural test sample 4 and water-sprayed test sample 2, and water-sprayed test samples 5 and 6 and natural test sample 1. (These pairings are for samples with similar weight proportions of rock.) Moreover, the maximum and minimum shear forces for sample 4, which had a lower weight proportion of rock, decreased more than that of test samples 5 and 6, which had a higher weight proportion of rock. Also, the decrease in cohesion for water-sprayed sample 4 was more than that for water-sprayed samples 5 and 6; nevertheless, the cohesion of all the water-sprayed test samples are very close. The internal friction angles of all the water-sprayed test samples increase greatly compared with those of the natural samples. The internal friction angle of test sample 4 was 57·74°, some 8·7° higher than test sample 2, which had a similar weight proportion of rock. Similarly, the internal friction angles of samples 5 and 6 increased by about 12·4° compared with sample 1, despite their similar weight proportions of rock. These phenomena may be explained as follows.

Water spraying changes the initial structure, disintegrating the structure of the soil fabric of the soil–rock mixture, and even piping fine grains. As a result, the bonding of soil between rock fragments weakens, and the soil–rock mixture becomes less coherent than in the drier state. The cohesion of the simulated rain soil–rock mixtures decreases markedly, especially for those for which the weight proportion of rock is small. The filling materials of the soil–rock mixtures facilitate shearing between the broken stones when in a natural condition. However, the softening and disintegration

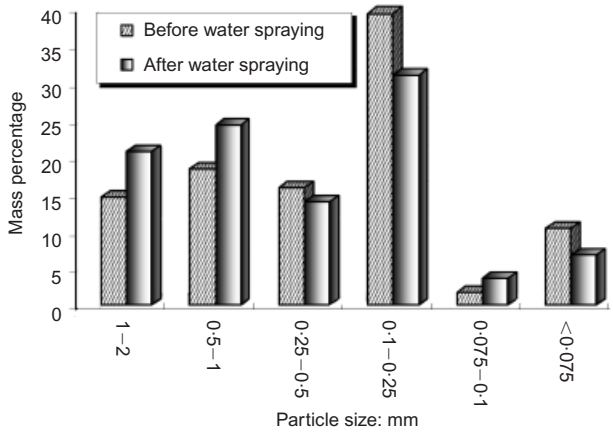

Fig. 12. Grain size distribution of test sample 4 before and after water spraying

of the filling materials allow the rock fragments to touch after water spraying, thus increasing the internal friction angle of the soil–rock mixture.

Test samples 5 and 6 are similar in both the grain size distribution and the maximum and minimum shear forces, but their shear stress–strain curves are significantly different. Based on the field investigation, test sample 6, which had many interspaces and whose density was less than that of test sample 5, was looser than test sample 5 and thus sustained a longer compaction stage.

Analyses of sliding surfaces. In order to better understand the deformation and failure mechanism of the soil–rock mixtures, a shear force was again applied to the test samples two days after the tests. Following initial displacement in this subsequent test, the upper sliding body was removed, and the 3D sliding surface observed. Using a distribution of measuring points, the 3D surfaces were analysed by computer. Results for test samples 1 and 3 are shown in Fig. 6, as examples.

Observation of the sliding surfaces shows that their smoothness and uniformity depends upon the weight proportion of rock in the soil–rock mixture. For example, sample 3 with fewer rock fragments has a smoother and more regular sliding plane than test sample 1, which has a higher weight proportion of rock, and a rougher, or more irregular, sliding plane. Clearly, the weight proportion of rock and the particle size distribution of the soil–rock mixture are important in controlling the mechanical character, and perhaps also the formation and shape, of the sliding surfaces. Also, the shapes of the broken stones in this area are very irregular, as they consist mainly of sandstones. These factors combine to increase the internal friction angle of the soil–rock mixtures in this area.

Soil–rock mixtures are heterogeneous, which leads to irregularity across the samples of the sliding surfaces. Thus average sliding surfaces computed as the mean of the profiles were selected as the characteristic sliding surface for calculation of the strength parameters.

Finally, during testing it was observed that most sliding surfaces negotiated around bigger sandstone fragments, and only a few passed through the weaker slate fragments.

CONCLUSIONS

Prior to this study, no data were available on in situ deformation of the soil–rock mixtures in the Hutiao Gorge area. Although the tests reported here are limited, they at least provided the following information.

(*a*) The tests gave valuable information on the strength parameters for the soil–rock mixtures in the study area: for natural soil–rock mixtures the cohesion c is 1·53 kPa and the internal friction ϕ is 46·0°; for simulated rain soil–rock mixtures c is 0·30 kPa and ϕ is 59·2°.

(*b*) The strength characteristics of soil–rock mixtures are closely related to their weight proportion of rock, although when the weight proportions of rock are similar, strength, and especially cohesion, may be influenced by some critical grain sizes. It is important to determine the particle size distribution of in situ soils when appraising the strength of soil–rock mixtures.

(*c*) Strength tests of the soil–rock mixture under natural conditions in the test area produced an irregular-shaped stress–strain curve with an 'S' shape. At the beginning of the test the soil undergoes a compaction stage, and before the ultimate strength is reached there is a longer stage of initial yielding and stress-hardening. The length of this stage depends on the proportion of rock, and is very different from that of pure soil or pure rock.

(*d*) Soil–rock mixtures are very sensitive to water. The cohesion of soil–rock mixtures under simulated rain conditions decreases sharply relative to that of the natural material, but the internal friction angle increases. This behaviour may decrease with an increase in the weight proportion of rock.

(*e*) Analyses of the 3D sliding surfaces reveal the significant contribution of the rock fragments in controlling the deformation and failure mechanism of the soil–rock mixture, and in controlling the formation of the sliding surfaces.

ACKNOWLEDGEMENTS

The work presented in this paper was supported by the Innovation Programme of the Chinese Academy of Sciences (Project No. KZCX3-SW-134), and the Chinese National Programme of Basic Research (Project 973, No. 2002CB412702).

REFERENCES

He, J.-Ming. (2004). *Study of deformation and failure mechanisms of soil/rock mixtures in Three Gorges reservoir area.* PhD dissertation. China University of Mining and Technology (Beijing).

Iannacchione, A. T. (1997). *Shear strength of saturated clays with floating rock particles.* PhD dissertation, University of Pittsburgh.

Li, S.-H. & Wang, Y.-N. (2004). Stochastic model and numerical simulation of uniaxial loading test for rock and soil blending by 3D-DEM. *Chin. J. Geotech. Engng* **26**, No. 2, 172–177 (in Chinese).

Lin, Z. (1994). *Geotechnical testing and monitoring manual.* Shenyang: Liaoning Science and Technology Publishing House (in Chinese).

Lindquist, E. S. & Goodman, R. E. (1994). Strength and deformation properties of a physical model melange. *Proc. 1st North American Rock Mechanics Conf. (NARMS), Austin, TX*, 843–850.

Medley, E. W. (1994). *Engineering characterization of melanges and similar block-in-matrix rocks (bimrocks).* PhD dissertation, Department Civil Engineering, University of California at Berkeley.

Medley, E. W. & Lindquist, E. S. (1995). The engineering significance of the scale-independence of some Franciscan mélanges in California, USA. *Proc. 35st US Rock Mechanics Symp.*, Reno, 907–914.

Vallejo, L. E. (2001). Interpretation of the limits in shear strength

in binary granular mixtures. *Can. Geotech. J.* **38**, No. 5, 1097–1104.

Vallejo, L. E. & Mawby, R. (2000). Porosity influence on the shear strength of granular material–clay mixtures. *Engng Geol.* **58**, No. 2, 125–136.

Vallejo, L. E. & Zhou, Y. (1994). The mechanical properties of simulated soil–rock mixtures. *Proc. 13th Int. Conf. Soil Mech. Found. Engng, New Delhi* **1**, 365–368.

Xia, Y. & Zhu, R. (1996). Study on sliding mechanism and stability evaluation for Xintan landslide in three gorges of the Changjiang river. *Chin. J. Geol. Hazard and Control* **7**, No. 3, 49–54 (in Chinese).

Xu, W. & Hu, R. (2006). Particle size fractal characteristics of the soil–rock mixtures in the right bank slope of Jinsha River at Long-Pan, Tiger-Leaping Gorge area, China. *J. Engng Geol.* **14**, No. 4, 496–501 (in Chinese).